Roles of Interfacial Modifiers in Hybrid Solar Cells: Inorganic/Polymer Bilayer vs Inorganic/Polymer:Fullerene Bulk Heterojunction

ARTICLE *in* ACS APPLIED MATERIALS & INTERFACES · DECEMBER 2013

Impact Factor: 6.72 · DOI: 10.1021/am402684w · Source: PubMed

7 AUTHORS, INCLUDING:

Liang Yan
University of North Carolina at Chapel Hill
31 PUBLICATIONS **381** CITATIONS
SEE PROFILE

Shubin Liu
University of North Carolina at Chapel Hill
155 PUBLICATIONS **5,513** CITATIONS
SEE PROFILE

Wei You
University of North Carolina at Chapel Hill
81 PUBLICATIONS **4,359** CITATIONS
SEE PROFILE

ACS APPLIED MATERIALS & INTERFACES

Research Article

www.acsami.org

Roles of Interfacial Modifiers in Hybrid Solar Cells: Inorganic/Polymer Bilayer vs Inorganic/Polymer:Fullerene Bulk Heterojunction

Seung Hun Eom,[†] Myung-Jin Baek,[†] Hanok Park,[†] Liang Yan,[‡] Shubin Liu,[§] Wei You,*[,‡] and Soo-Hyoung Lee*[,†]

[†]School of Semiconductor and Chemical Engineering, Chonbuk National University, 567 Baekje-daero, Deokjin-gu, Jeonju-si, Jeollabuk-do 561-756, Republic of Korea

[‡]Department of Chemistry, University of North Carolina at Chapel Hill, Chapel Hill, North Carolina 27599-3290, United States

[§]Research Computing Center, University of North Carolina at Chapel Hill, Chapel Hill, North Carolina 27599-3420, United States

Supporting Information

ABSTRACT: Hybrid solar cells (HSCs) incorporating both organic and inorganic materials typically have significant interfacial issues which can significantly limit the device efficiency by allowing charge recombination, macroscopic phase separation, and nonideal contact. All these issues can be mitigated by applying carefully designed interfacial modifiers (IMs). In an attempt to further understand the function of these IMs, we investigated two IMs in two different HSCs structures: an inverted bilayer HSC of ZnO:poly(3-hexylthiophene) (P3HT) and an inverted bulk heterojunction (BHJ) solar cell of ZnO/P3HT:[6,6]-phenyl C_{61}-butyric acid methyl ester (PCBM). In the former device configuration, ZnO serves as the *n*-type semiconductor, while in the latter device configuration, it functions as an electron transport layer (ETL)/hole blocking layer (HBL). In the ZnO:P3HT bilayer device, after the interfacial modification, a power conversion efficiency (PCE) of 0.42% with improved V_{oc} and FF and a significantly increased J_{sc} was obtained. In the ZnO/P3HT:PCBM based BHJ device, including IMs also improved the PCE to 4.69% with an increase in V_{oc} and FF. Our work clearly demonstrates that IMs help to reduce both the charge recombination and leakage current by minimizing the number of defect sites and traps and to increase the compatibility of hydrophilic ZnO with the organic layers. Furthermore, the major role of IMs depends on the function of ZnO in different device configurations, either as *n*-type semiconductor in bilayer devices or as ETL/HBL in BHJ devices. We conclude by offering insights for designing ideal IMs in future efforts, in order to achieve high-efficiency in both ZnO:polymer bilayer structure and ZnO/polymer:PCBM BHJ devices.

KEYWORDS: *hybrid solar cell, interfacial modifier, inverted structure, zinc oxide, organic−inorganic interface, charge recombination, work function*

1. INTRODUCTION

Both material design and fabrication techniques for polymer solar cells (PSCs) have rapidly advanced in recent years.[1−3] Power conversion efficiencies (PCEs) of 7−9% can now be routinely obtained for single junction PSCs.[4−8] While further improvement in PCEs is certainly needed to reach over 10% in the modules for commercial energy applications, other important factors pertinent to the commercial success, such as the high cost associated with the fullerene molecules and the stability of these organic devices, have received increasing amount of attention. For example, to replace fullerene molecules, typically used as *n*-type semiconductors in the PSCs, other *n*-type inorganic materials, such as CdSe, Si, TiO_2, and ZnO, have been used with *p*-type polymers to form hybrid solar cells (HSCs). The primary motivation is to take advantage of the high electron mobility of the inorganic nanomaterials to overcome charge-transport limitations typically associated with organic materials. Furthermore, these HSCs are morphologically more stable than polymer:fullerene based cells.[9−14] On the other hand, these *n*-type inorganics are frequently used in bulk heterojunction (BHJ) solar cells to render an "inverted" device configuration. This special type of HSCs offers long-term stability, achieved by replacing the low work function metal cathodes (e.g., Ca),[15,16] and by avoiding the highly corrosive and hydroscopic hole transporting material, poly(3,4-ethylenedioxythiophene):poly(styrenesulfonic acid) (PEDOT:PSS). Moreover, these inverted cells are still amenable to large-scale roll to roll processing,[17,18] and their active layer tends to have vertical phase separation, which helps reduce charge carrier recombination.[19]

However, several issues remain for HSCs. For example, the backflow of charge carriers and charge recombination at the organic−inorganic interface can lead to a decrease in short-circuit current density (J_{sc}), open-circuit voltage (V_{oc}), and fill

Received: July 10, 2013
Accepted: December 18, 2013
Published: December 18, 2013

factor (FF) in HSCs. In addition, the lack of compatibility between inorganic *n*-type layer (e.g., hydrophilic metal oxides) and *p*-type organic layer (e.g., hydrophobic polymers) can cause macroscopic phase separation and nonideal interfacial contact.[20] Therefore, inserting an interfacial modifier at the inorganic−organic interface has been actively pursued as an effective approach for overcoming these interfacial problems and achieving lower contact resistance, as well as reducing losses due to charge recombination.[21−24] For example, after modifying the poly(3-hexylthiophene) (P3HT)/TiO_2 interface with conjugated cyanoacrylic acid derivatives, Wang et al. observed a dramatic increase in the J_{sc} and V_{oc} of their hybrid solar cells where P3HT is infiltrated into the mesoporous TiO_2 layer.[25] In another earlier study, Su et al. also observed similar enhancement after they inserted an amphiphilic interfacial modifier inbetween the TiO_2 nanorods and the P3HT in a bulk heterojunction (BHJ) based hybrid solar cell.[26] In addition, when these inorganic *n*-type materials (e.g., TiO_2, ZnO) are used as the electron-transport layer (ETL)/hole-blocking layer (HBL) for polymer:fullerene based inverted BHJ cells, attaching interfacial modifiers on top of these inorganics has been shown to improve the device efficiency.[27−29] Nevertheless, a systematic study, comparing the effect of the same interfacial modifiers on both HSCs where inorganics serve as the *n*-type semiconductor and also inverted BHJ cells where the same inorganics function as ETL/HTL, is missing. Such a comparative study would further our understanding of how these interfacial modifiers function in different device configurations and facilitate the future design of such modifiers, which may be specific to a particular device configuration.

Herein, we intend to report such a comparative study. We chose ZnO as the *n*-type inorganic material because ZnO is one of the most commonly used *n*-type buffer layers in the inverted BHJ cells[30,31] and also is a very promising *n*-type semiconductor to replace [6,6]-phenyl C61-butyric acid methyl ester ($PC_{61}BM$).[32] We then synthesized two different interfacial modifiers (IMs) following the "donor−acceptor" design concept but with different chemical structures and energy levels. These IMs were used to modify the interfaces in the solar cells in two different places: (i) in between ZnO and P3HT where ZnO serves as an inorganic acceptor and P3HT functions as an organic donor in an inverted bilayer HSC and (ii) on top of ZnO which functions as an inorganic HBL/ETL in an inverted BHJ solar cell, where P3HT:[6,6]-phenyl C_{61}-butyric acid methyl ester (PCBM) is used as the organic photoactive layer (Figure 2). In the ZnO:P3HT inverted bilayer HSC, the surface modification of ZnO with IMs exhibited enhanced PCEs with significantly improved J_{sc} when compared to the unmodified devices. For ZnO/P3HT:PCBM inverted BHJ devices, we also observed improved PCEs, mainly due to the enhanced FF and V_{oc}. These results demonstrate that in both structures IMs serve similar functions of (a) reducing the number of defect sites and traps on the ZnO surface and (b) increasing the compatibility of hydrophilic ZnO with the organic layers. More importantly, the major role of IMs depends on whether ZnO functions as *n*-type semiconductor or as ETL/HBL in a different device configuration.

2. EXPERIMENTAL SECTION

2.1. Materials and Synthesis. *N*-Bromosuccinimide, triphenyl boronic acid, $Pd(PPh_3)_4$, tricyclohexylphosphine, 20% aqueous tetraethylammonium hydroxide, tributyl(thiophen-2-yl)stannane, $POCl_3$, *N*,*N*-dimethylformamide (DMF), cyanoacetic acid, and piperidine were all purchased from Aldrich. $Pd_2(dba)_3$ and tri(o-tolyl) phosphine were purchased from Strem. All solvents used were analytical grade. The detailed synthetic routes and procedures for the IM1 and IM2 are shown in Scheme S1 and described in the Supporting Information.

2.2. General Instrumentation. ^1H and ^{13}C NMR spectra were recorded on a JEOL FT-NMR (400 MHz) spectrophotometer using $CDCl_3$ as the solvent. Chemical shifts were reported as δ values (ppm) relative to the internal standard tetramethylsilane (TMS). The UV−vis absorption spectra were obtained using a V-670 (JASCO) spectrophotometer. Cyclic voltammetry (CV) measurements were performed on a VersaSTAT3 (METEK) under argon at a scan rate of 50 mVs^{-1} at room temperature, wherein a Pt wire and Ag/AgCl were used as the counter and reference electrodes, respectively. The reference electrode was calibrated with Fc/Fc^+ as the external standard. The samples were prepared in a chloroform solution with 0.10 M tetrabutylammonium hexafluorophosphate ($n\text{-}Bu_4NPF_6$) as the electrolyte.

2.3. Photovoltaic Device Fabrication and Characterization. All photovoltaic cells were prepared on a commercial indium tin oxide (ITO)-coated glass substrate. Prior to use, the patterned ITO-covered glass substrates were cleaned with deionized water, acetone, and isopropyl alcohol by ultrasonication, followed by treatment with a UV−ozone cleaner for 12 min. ZnO precursor was prepared by dissolving zinc acetate (Aldrich, 99.9%, 1 g) and ethanolamine (Aldrich, 99.5%, 0.28 g) in 2-metahoxyethanol (Aldrich, 99.8%, 10 mL) under stirring for 12 h in the air. The ZnO precursor solution was then spin-coated (6000 rpm, 60 s) onto the previously cleaned ITO-glass with a thickness of 20−23 nm and dried at 200 °C for 10 min in air. Samples for interfacial modification (both bare ITO and ZnO functionalized substrates) were then dipped in 0.5 mM solutions of IMs in THF for 60 s, then rinsed with THF for 5 min, and finally dried under N_2 flow. Different dipping times and solution concentrations of IMs were used to find optimized coverage of IMs on the surface of ZnO. Dipping time of 60 s in 0.5 mM solution showed the largest absorption intensity and the best device performance with small standard deviations for both IMs (see Figure S7 of the Supporting Information). Blends of P3HT and PCBM (Nano-C, USA) with 1:1 weight ratio or pure P3HT were dissolved in *o*-dichlorobenzene (ODCB) with a concentration of 30 mg/mL, filtered through a 0.45 μm poly(tetrafluoroethylene) (PTFE) filter, and subsequently spin-coated at 400 rpm for 60 s onto the ZnO layer on ITO. The thickness for P3HT:PCBM blend based film was measured to be 230 nm, while 300 nm was determined for P3HT only film. The resulting films were dried in sealed Petri dishes for 8 h under nitrogen in the glovebox. The devices were completed by depositing a 10 nm layer of MoO_3 and a 100 nm layer of Ag. These layers were thermally evaporated at a pressure of 1×10^{-6} Torr with a shadow mask. The active area of every device was 0.12 cm^2. The current density−voltage (J−V) characteristics of the photovoltaic devices were measured with a Keithley 2400 source-measure unit in the dark and under 100 mW/cm^2 AM 1.5G condition with a solar simulator (Oriel 91160, 300 W), calibrated with a monocrystalline silicon solar cell as the standard PV reference (2 × 2 cm, calibrated at NREL, Colorado, USA).

3. RESULTS AND DISCUSSION

3.1. Synthesis and Characterization of IM1 and IM2. Typically, each IM molecule includes an end functional group (e.g., carboxylic acid, phosphonic acid) that allows the IM to be covalently attached to the substrate (e.g., metal oxides). In our study, we chose carboxylic acid (−COOH) as the linked to attach these IMs to ZnO. Next, we added an electron-withdrawing moiety (cyano) on the side of the anchoring group to direct the molecular dipole in the right direction, i.e., away from ZnO. Please note that the dipole direction is defined as pointing from the negative pole to the positive pole.[22,25,33,34] To maintain the dipole direction, the remaining structural units are typically electron-rich organic conjugated groups (e.g.,

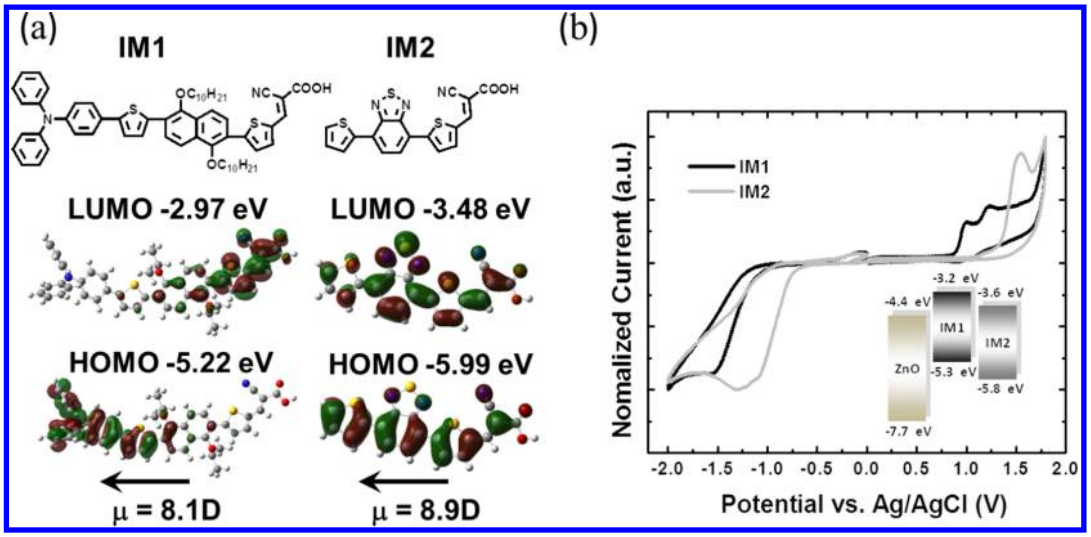

Figure 1. (a) Chemical structures, the optimized geometry, the electron density distributions, and the HOMO and LUMO energy levels of IMs and (b) cyclic voltammograms of IMs (Inset: Energy level diagram showing the HOMO and LUMO energy levels of IMs and ZnO by the CV measurement).

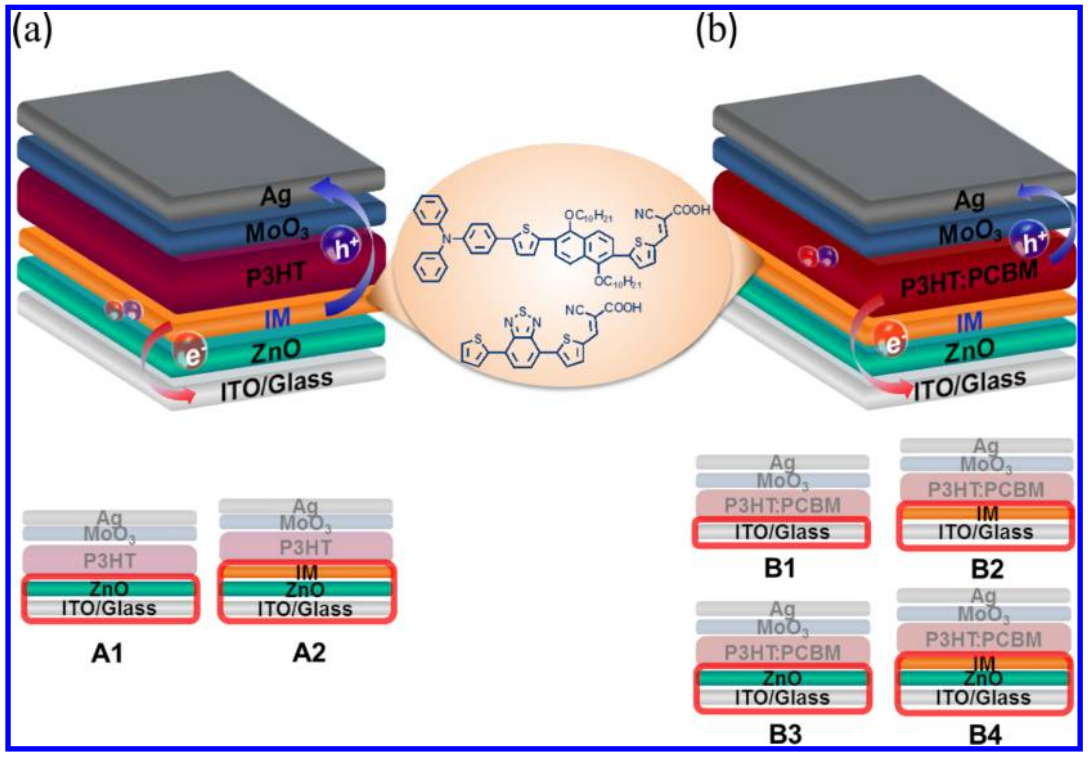

Figure 2. The basic device structures of hybrid solar cells in this study: (a) ZnO:P3HT bilayer structure and (b) P3HT:PCBM BHJ structure with ZnO as ETL/HBL. Bottom pictures show six difference solar cell configurations (Devices A1-A2 and B1-B4) with and without IMs based on the basic device structures.

benzene, thiophene, fluorene). For example, a combination of substituted naphthalene, thiophene, and triphenyl amine constitute the aromatics for IM1 in our study. The structure of IM1 is shown in Figure 1a, together with IM2, an effective IM that was previously used for TiO_2.[25] The differing structures of the aromatics in these two IMs should lead to significantly different energy levels (i.e., highest occupied molecular orbital, HOMO, and lowest unoccupied molecular orbital, LUMO), band gap, and dipole moments. Therefore, these two IMs would constitute an appropriate pair for comparative study.

Prior to the synthesis, we performed density functional theory (DFT) calculations to obtain the optimized structure, the electron density distributions, and HOMO and LUMO energy levels for these two IMs. The calculations were carried out at the B3LYP/6-311+G* level of theory. All quantum mechanical calculations have been carried out using Gaussian 09 version B.01 package[35,36] with no symmetry constraint, tight self-consistent field (SCF) convergence criteria, and ultrafine integration grids. After a full geometry optimization, a single point frequency calculation was performed to verify that the structures obtained were indeed a minimum on the potential

dx.doi.org/10.1021/am402684w | ACS Appl. Mater. Interfaces 2014, 6, 803−810

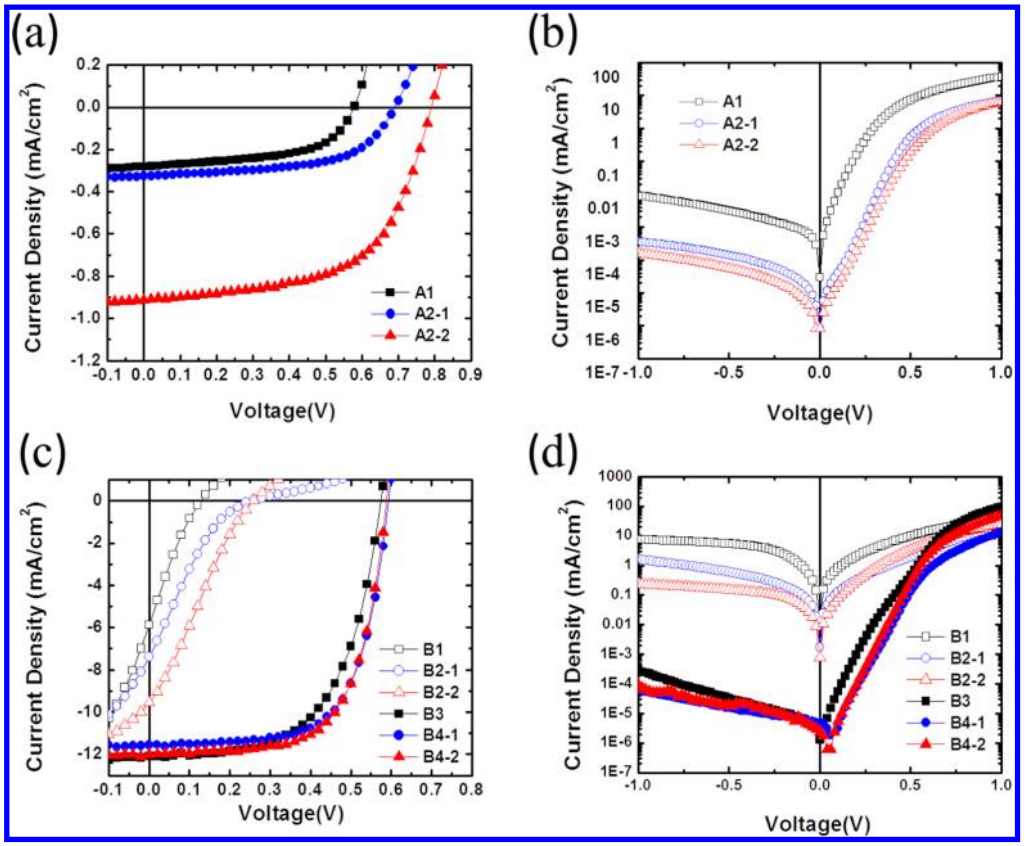

Figure 3. *J*–*V* curves of ZnO:P3HT bilayer hybrid solar cells with IMs under (a) illumination and (b) dark conditions. A1: ITO/ZnO:P3HT; A2-1: ITO/ZnO/IM1:P3HT; A2-2: ITO/ZnO/IM2:P3HT. *J*–*V* curves of P3HT:PCBM BHJ hybrid solar cells with IMs (c) under illumination and (d) dark conditions. B1: ITO/P3HT:PCBM; B2-1: ITO/IM1/P3HT:PCBM; B2-2: ITO/IM2/P3HT:PCBM; B3: ITO/ZnO/P3HT:PCBM; B4-1: ITO/ZnO/IM1/P3HT:PCBM; B4-2: ITO/ZnO/IM2/P3HT:PCBM.

Table 1. Photovoltaic Characteristics of Hybrid Solar Cells

device structure	J_{sc} (mA/cm^2)[a]	V_{oc} (V)[a]	FF (%)[a]	PCE (%)[a]	R_{sh} (Ω·cm^2)	R_s (Ω·cm^2)
(A1) ITO/ZnO:P3HT	0.20 (0.27)	0.57 (0.57)	56.74 (56.71)	0.09 (0.09)	189.4	14.7
(A2-1) ITO/ZnO/IM1:P3HT	0.33 (0.29)	0.69 (0.71)	57.78 (56.96)	0.13 (0.12)	1027.9	58.9
(A2-2) ITO/ZnO/IM2:P3HT	0.91 (0.91)	0.79 (0.78)	58.63 (57.85)	0.42 (0.41)	1334.7	55.6
(B1) ITO/P3HT:PCBM	5.86 (5.15)	0.13 (0.12)	20.00 (19.80)	0.15 (0.12)	9.3	6.7
(B2-1) ITO/IM1/P3HT:PCBM	7.03 (6.55)	0.21 (0.24)	21.58 (17.43)	0.32 (0.27)	74.6	1.6
(B2-2) ITO/IM2/P3HT:PCBM	9.54 (9.17)	0.25 (0.26)	25.14 (22.81)	0.60 (0.55)	272.4	12.9
(B3) ITO/ZnO/P3HT:PCBM	12.09 (11.78)	0.57 (0.57)	59.79 (60.01)	4.12 (3.96)	957.8	2.8
(B4-1) ITO/ZnO/IM1/P3HT:PCBM	11.56 (11.18)	0.59 (0.59)	66.74 (65.15)	4.55 (4.30)	2078.2	18.9
(B4-2) ITO/ZnO/IM2/P3HT:PCBM	11.87 (11.46)	0.59 (0.59)	66.96 (64.09)	4.69 (4.33)	2172.4	5.4

[a]Average values are in parentheses.

energy surface (e.g., no imaginary frequency). As shown in Figure 1a, the optimized geometry of IM2 has the thiophene-benzothiadiazole-thiophene unit coplanar with respect to the cyanoacrylic acid group, indicating good conjugation across the entire molecule. In the optimized geometry of IM1, on the other hand, the triphenyl amine group is tilted slightly from the coplanar backbone of thiophene-naphthalene-thiophene-cyanoacrylic acid. This leads to a less effective conjugation in IM1 as compared to the more effective conjugation through thiophene-benzothiadiazole-thiophene (D-A-D) in the case of IM2. This less effective conjugation of IM1partially accounts for its slightly larger band gap. The decrease in effective conjugation for IM1 also explains why the electron density of the HOMO is localized on the triphenyl amine in IM1, in contrast to the more delocalized electron density of the HOMO in IM2. Similarly, the electron density of the LUMO in IM1 is localized near the cyanoacrylic acid, while the LUMO of IM2 has an electron density spreading across the entire molecule due to the incorporation of the electron-withdrawing benzothiadiazole between the thiophene units. We also estimated the intrinsic dipole moments (μ) of both IMs by DFT calculation (Figure 1a). The slightly larger μ value of IM2 than that of IM1 can be ascribed to having additional electron-withdrawing benzothiadiazole in IM2, instead of the electron donor unit naphthalene in IM1, inserted between the two thiophene units.

Figure 1a also shows that both the HOMO and the LUMO energy levels of IM2 are lower than those of IM1, likely due to the incorporation of electron-withdrawing benzothiadiazole in the D-A-D backbone of IM2. Cyclic voltammetry (CV)

dx.doi.org/10.1021/am402684w | ACS Appl. Mater. Interfaces 2014, 6, 803–810

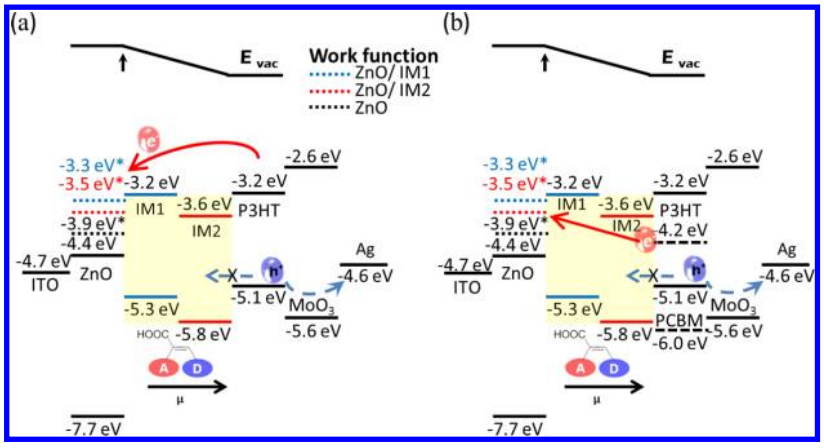

Figure 4. Detailed energy level diagrams and charge transfer processes of (a) ZnO:P3HT bilayer hybrid solar cells with IMs and (b) ZnO/P3HT:PCBM BHJ hybrid solar cells with IMs [−4.4 eV is the reported work function value of ZnO (ref 31); ∗, work function values by UPS].

experimentally confirmed the higher HOMO and LUMO levels of IM2, which were calculated according to the formula HOMO = $-(E^{ox}_{onset} + 4.4)$ eV and LUMO = $-(E^{red}_{onset} + 4.4)$.[37] From the cyclic voltammograms of both IM1 and IM2 (Figure 1b), the onset oxidation potentials for IM1 and IM2 are estimated to be around 0.89 and 1.35 V, respectively, versus the Ag/AgCl reference electrode. These values correspond to HOMO energy levels of −5.29 and −5.75 eV for IM1 and IM2, respectively. On the other hand, the LUMOs of IM1 and IM2 are estimated to be −3.23 and −3.64 eV, respectively, based on the onset reduction potentials at −1.17 V (IM1) and −0.76 V (IM2). We then constructed a comparative energy diagram including both IMs and ZnO, presented as the inset of Figure 1b.

3.2. Photovoltaic Devices and Characteristics. Figure 2 shows the two device structures we employed in this study. A solution processed ZnO thin layer was applied onto the ITO substrate in both device structures. However, in the bilayer structure (Figure 2a), ZnO serves as the *n*-type acceptor, whereas in the inverted BHJ solar cells (Figure 2b), ZnO is used as the HBL/ETL.

ZnO:P3HT Bilayer Solar Cell. Figure 3a,b compares current density−voltage (J−V) curves of ZnO:P3HT bilayer HSCs under illumination and dark conditions, respectively. The detailed device characteristics are also summarized in Table 1. Not surprisingly, the device fabricated without IMs (Device A1) exhibits very poor performance with a PCE of 0.09%, due mainly to a very small J_{sc}. We offer two reasons to account for the observed small J_{sc}. First, poor interfacial contact, due to the hydrophilic nature of ZnO (see low contact angle value in Figure S8a of the Supporting Information) and the hydrophobic P3HT, leads to inefficient splitting of the photogenerated excitons and results in the small photocurrent (J_{ph}). Second, the poor diode of ZnO:P3HT leads to a very large dark current under reverse bias (Figure 3b), which can further decrease the obtained J_{sc} value in the device.

Fortunately, both the poor interfacial contact and the poor diode behavior of ZnO:P3HT are significantly rectified by the interfacial modification of the ZnO surface with IMs, leading to much improved V_{oc} and J_{sc} values, while still maintaining a decent FF (Figure 3a and Table 1). For example, the devices fabricated with IM1 (Device A2-1) and IM2 (Device A2-2) both present a significantly improved V_{oc} of 0.69 and 0.79 V, respectively, much higher than that of the device without IMs (0.57 V). Previous studies of similar systems (e.g., TiO_2:polymer bilayer solar cells) have shown that the maximum attainable V_{oc} in such systems is strongly associated with the band edge difference between the conduction band level (E_{CB}) of metal oxides (e.g., TiO_2) and the HOMO level (E_{HOMO}) of the polymer.[38] A larger E_{CB}−E_{HOMO} gap would then lead to a higher V_{oc}. In our studied system, the work function of ZnO increases after the IM modification, from −3.9 eV (ZnO) to −3.3 eV (ZnO/IM1) and −3.5 eV (ZnO/IM2), respectively, as measured by ultraviolet photoemission spectroscopy (UPS) (Figure 4a). The increased work function of ZnO is likely caused by the IM molecules on ZnO creating a thin layer of dipoles pointing away from the ZnO surface, thereby shifting the conduction band edge of ZnO (which is close to the absolute value of E_{CB} of ZnO) upward. This would consequently raise the ZnO_{CB}−$P3HT_{HOMO}$ gap and result in the higher V_{oc} values of Device A2-1 and Device A2-2.

Though a higher conduction band level value was obtained for ZnO/IM1 (−3.3 eV) than for ZnO/IM2 (−3.5 eV), the observed V_{oc} of Device A2-1 (0.67 V) is surprisingly smaller than that of Device A2-2 (0.79 V). This rather unexpected observation, i.e., a smaller V_{oc} of Device A2-1 with a larger ZnO_{CB}−$P3HT_{HOMO}$ gap, can be partly explained by the larger leakage current measured in the ZnO/IM1 interface as shown in Figure 3b. A large reverse saturation current, the "leakage" current, usually leads to a V_{oc} lower than the value predicted by the Donor/Acceptor interface energy gap (i.e., ZnO_{CB}−$P3HT_{HOMO}$ in our study).[39,40] Concerning why the ZnO/IM1 interface creates a larger leakage current in its device, we offer two possible explanations. First, the HOMO level of IM1 (−5.3 eV) is very close to the HOMO of P3HT (−5.1 eV). This would still allow holes to pass through the IM1 layer, while the much deeper HOMO value of IM2 can block holes effectively. These "leaked" holes can then recombine with electrons at the ZnO (with IMs) and P3HT interface, leading to a large leakage current. Second, the steric hindrance from the bulky triphenyl amine units of IM1 could render insufficient IM1 surface coverage on the ZnO, which could also contribute to the large leakage current.[41]

Although attaching IM1 to the surface of ZnO increases the V_{oc} of Device A2-1, the J_{sc} of the device is only slightly improved when compared with the unfunctionalized ZnO:P3HT bilayer device. We believe that the exciton dissociation at the interface of P3HT and IM1 functionalized ZnO is not efficient. Typically, the energy difference between the LUMO levels of the donor (i.e., P3HT in our study) and

acceptor (i.e., ZnO) should be greater than 0.3 eV to overcome the exciton binding energy and to ensure efficient electron transfer.[42] In our study, the work function of ZnO/IM1 (−3.3 eV) is very similar to the LUMO of P3HT (−3.2 eV). Such a small difference (∼0.1 eV) cannot provide enough driving force to promote the effective dissociation of excitons. On the other hand, switching to IM2 noticeably decreases the work function of ZnO/IM2 to −3.5 eV, which can certainly facilitate the exciton splitting with a larger driving force (∼0.3 eV). Additionally, IM2 has a much lower HOMO energy level (−5.8 eV), which blocks the leaking of holes more effectively than IM1 can. A smaller leakage current in the case of the ZnO/IM2 based Device A2-2 also explains the higher J_{sc} than that of the ZnO/IM1 based Device A2-1. The difference in the leakage current can also help explain the higher FF observed in the case of ZnO/IM2 based Device A2-2 (Table 1). In summary, with an improved V_{oc} and FF and a significantly increased J_{sc}, the IM2 modified device (Device A2-2) exhibits the best PCE of 0.42%, which triples that of the IM1 modified device (Device A2-1).

ZnO/P3HT:PCBM BHJ Solar Cell. When the same ZnO layer is used as the HBL/ETL in inverted BHJ solar cells, the same IMs used in the previous bilayer devices have a different impact on the device. Figure 2b schematically shows all BHJ device configurations studied. All $J-V$ curves of these devices under illumination and dark conditions are shown in Figure 3c,d, respectively, with related device characteristics listed in Table 1.

Not surprisingly, the ITO-only device (Device B1) exhibits very poor performance with a PCE of ∼0.15%. With IMs, the performance of both devices (Device B2-1 and Device B2-2) was noticeably improved, showing better J_{sc}, V_{oc}, and FF values than those of Device B1. These results indicate that IMs can help to suppress the charge recombination and leakage current occurring at the interface between the ITO electrode and the P3HT:PCBM active layer. This assessment is supported by the smaller dark current density values of both IM-added devices than that of the ITO-only device (B2-1 and B2-2 vs B1 in Figure 3d). Nevertheless, all three devices, including the IM-added ones, show S-shaped curves, indicating that surface charge recombination is still a significant energy loss mechanism even after the inclusion of IMs between the ITO and the P3HT:PCBM active layer. This is likely due to incomplete IM coverage of the active layer as a result of the simple dipping method we employed. Such incomplete coverage may stem from two possible sources: (a) the density of hydroxyl groups on the ITO surface is quite low and (b) the carboxyl groups of IMs could not be fully coupled with these surface hydroxyl groups by this simple dipping method. This indicates that an alternative or additional interfacial layer is needed in order to minimize various surface-related energy loss effects (e.g., surface charge recombination) and maximize the device efficiency.

Fortunately, a sol−gel-derived ZnO thin film shows promise as such an interfacial layer. With aconduction band level of −4.4 eV and a valence band of −7.7 eV, the band structure of ZnO is well-matched with the energy levels of organic donors, thereby facilitating electron transport and hole blocking between the photoactive layer and the cathode. For example, ZnO has been employed as an effective *n*-type buffer layer in inverted polymer BHJ solar cells.[31] Indeed, after we applied sol−gel-derived ZnO film between the ITO and photoactive layer, the device (Device B3) demonstrates a dramatically improved PCE, reaching 4.12% with a J_{sc} of 12.09 mA/cm^2, a V_{oc} of 0.57 V, and a FF of 59.8%. However, like ITO, the surface of ZnO is hydrophilic due to the presence of surface hydroxyl groups, which could cause charge trapping at the interface with the hydrophobic P3HT:PCBM photoactive layer. In addition, the incompatibility between the inorganic ZnO and the organic layer may cause macroscopic phase separation and poor interfacial contact, which can contribute to a large leakage current by backflow of charge carriers and charge recombination at ZnO/organic interfaces. All of these scenarios would result in a low J_{sc}, V_{oc}, and FF in the inverted BHJ solar cells.[43] In order to mitigate these potential issues with the ZnO interfacial layer, we applied the same IMs to the surface of ZnO in our inverted BHJ cells, a practice we employed in the previous discussion of ZnO:P3HT bilayer devices. These additional results will complete our comparative study of how these interfacial modifiers function in different device configurations.

Indeed, these IM modified devices (Device B4-1 and Device B4-2) exhibit noticeable improvement in V_{oc} and FF (Figure 3c and Table 1), which can be ascribed to the following reasons. First, introducing the IM on the surface of ZnO converts the hydrophilic ZnO into a hydrophobic surface, evidenced by the increase of the contact angle after the IM modification (Figure S8, Supporting Information). The increased hydrophobicity of the IM-modified ZnO layer allows for a better interfacial contact with the organic active layer. In addition, IM functionalization can help minimize surface defects and dangling bonds, both of which could serve as charge traps. For these reasons, adding IMs on the surface of ZnO can help reduce the number of trap sites and minimize the leakage current. Second, without IM, the P3HT in the BHJ active layer could directly contact the ZnO surface, leading to increased charge recombination at the interface between ZnO and P3HT. When the IMs are present, their deep HOMO levels (−5.3 eV for IM1 and −5.8 eV for IM2), when compared with the HOMO of P3HT (−5.1 eV), can further prevent charge recombination at the ZnO/active layer (P3HT:PCBM) interface, thereby enhancing V_{oc} and FF in the IM modified devices. As a result, the IM1 and IM2 modified devices with ZnO as the buffer layer (Device B4-1 and B4-2) offer PCE up to 4.55% and 4.69%, respectively, a noticeable improvement over the PCE of 4.12% with the unmodified device (Device B3).

On the other hand, devices containing IM layers (Device B4-1 and Device B4-2) show slightly reduced J_{sc} values. This may be caused by the extra barrier for electron transport due to the high LUMO values of these IMs. As shown in Figure 4b, LUMO levels of IM1 (−3.2 eV) and IM2 (−3.6 eV) are higher than the LUMO of PCBM (−4.2 eV), indicating that both IMs may block the electron transport from PCBM to the ZnO/ITO.

3.3. Role of Interfacial Modifier in HSCs. Our comparative study of selected interfacial modifiers (IMs) in two different device configurations of hybrid solar cells (HSCs) allows us to identify the role of IMs in specific device configurations (Figure 5). From the above discussion, it becomes quite clear that the major role of IMs in each device is closely tied to the function of ZnO in different device configurations.

In ZnO:polymer bilayer devices, the core photovoltaic event, the *exciton dissociation*, occurs at the ZnO:polymer interface where ZnO is the *n*-type semiconductor and polymer is the *p*-type semiconductor. With a strong dipole enabled by the donor−acceptor structure and the proper orientation (i.e.,

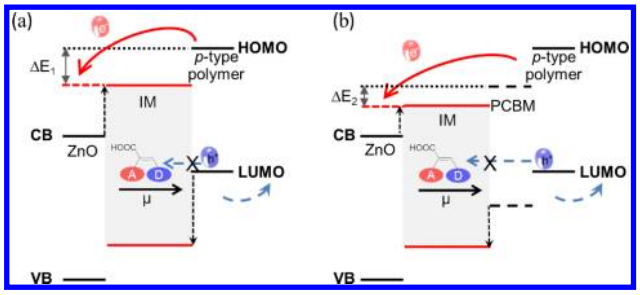

Figure 5. Designing ideal interfacial modifiers for high device efficiency in (a) ZnO:polymer bilayer hybrid solar cells and (b) ZnO/polymer:PCBM BHJ hybrid solar cells.

dipole moment pointing away from ZnO to the organic layer), the IM can lift the conduction band level of ZnO as much as 1.1 eV. This upward shift of the ZnO conduction band level has a strong impact on the V_{oc} of the ZnO:polymer bilayer device. For example, as shown in Table 1, the IM2-modified ZnO:P3HT bilayer device has a much higher V_{oc} than that of the pristine ZnO:polymer device (0.79 vs 0.57 V). However, there is a limit to the benefits of shifting the conduction band level of ZnO: too high a conduction band level will narrow the energy level difference in regard to the LUMO of the polymer (ΔE_1 in Figure 5a) and diminish the driving force for exciton splitting, leading to a smaller J_{sc} (e.g., comparing Device A2-1 with Device A2-2).

On the other hand, in ZnO/polymer:PCBM BHJ devices, ZnO mainly serves as the ETL/HBL, affecting the *electron transport*. In such devices, where the exciton dissociation happens at the polymer/PCBM interface, V_{oc} is essentially determined by the relative energy levels of the polymers and PCBM; therefore, ZnO and IMs mainly impact V_{oc} by controlling the leakage current. Because in this case the major role of ZnO is as an ETL/HBL, these IMs should have a LUMO energy level lower than that of PCBM (ΔE_1 in Figure 5a) to promote the electron transport; too high a LUMO level of the IM leads to a reduced J_{sc} (e.g., comparing Device B3 with Devices B4-1 and B4-2).

Finally, in both ZnO:polymer bilayer structure and ZnO/polymer:PCBM BHJ devices, attaching IMs on the surface of ZnO can minimize the number of defect sites and traps and increase the compatibility of originally hydrophilic ZnO with the organic polymers.

4. CONCLUSION

Our comparative study of two different interfacial modifiers (IMs) in two different device configurations clearly shows the benefits of employing these IMs in hybrid solar cells (HSCs) and offers helpful insights regarding the future design of ideal IMs (Figure 5). In ZnO:polymer bilayer devices, the ideal IM should elevate the conduction band level of ZnO to maximize the V_{oc} while still maintain the necessary driving force (0.3−0.5 eV) to effectively split the exciton and to allow a high J_{sc}. In ZnO/polymer:PCBM BHJ devices, the ideal IM should have a lower LUMO level than that of PCBM to allow effective electron transport. In both cases, a lower HOMO level of the IM, with its hole blocking properties, would be desirable to minimize the charge recombination and leakage current. Finally, all of these effects require complete coverage of IMs on the surface of ZnO and can only be achieved by appropriately designing these IMs.

It is worth noting that a simple treatment of ZnO surface with IM2 dramatically increased the efficiency of ZnO/polymer bilayer devices from 0.09% to 0.42%, an improvement over 300%! The efficiency-limiting factor of such devices is the J_{sc} (less than 1 mA/cm^2), likely due to the limited interfacial area (intrinsic to this bilayer design). Therefore, creating a bulk-heterojunction like device would in principle solve this issue and lead to an improved J_{sc} (and thereby higher efficiency) for these PCBM-free hybrid solar cells.[32]

■ ASSOCIATED CONTENT

Ⓢ Supporting Information

Synthetic schemes and procedures for the IM1 and IM2, the NMR and FT-IR spectra of IMs, the absorption spectra of IMs, and the contact angles of ZnO and ZnO/IMs. This information is available free of charge via the Internet at http://pubs.acs.org/.

■ AUTHOR INFORMATION

Corresponding Authors

*E-mail: wyou@unc.edu.
*E-mail: shlee66@jbnu.ac.kr.

Notes

The authors declare no competing financial interest.

■ ACKNOWLEDGMENTS

We acknowledge support from Basic Science Research Program (2011-0013277) through NRF funded by MEST, Korea, and a NSF SOLAR Grant (DMR-1125803). S.-H. Lee is grateful to the LG Yonam Foundation for the visiting professorship.

■ REFERENCES

(1) Na, S.-I.; Kim, S.-S.; Jo, J.; Kim, D.-Y. *Adv. Mater.* **2008**, *20*, 4061.
(2) Park, H. J.; Kang, M. G.; Ahn, S. H.; Guo, L. J. *Adv. Energy Mater.* **2010**, *22*, E247.
(3) Yang, L.; Zhang, T.; Zhou, H.; Price, S. C.; Wiley, B. J.; You, W. *ACS Appl. Mater. Interfaces* **2011**, *3*, 4075.
(4) Liang, Y.; Xu, Z.; Xia, J.; Tsai, S. T.; Wu, Y.; Li, G.; Ray, C.; Yu, L. *Adv. Energy Mater.* **2010**, *22*, E135.
(5) Huo, L.; Zhang, S.; Guo, X.; Xu, F.; Li, Y.; Hou, J. *Angew. Chem., Int. Ed.* **2011**, *50*, 9697.
(6) Price, S. C.; Stuart, A. C.; Yang, L.; Zhou, H.; You, W. *J. Am. Chem. Soc.* **2011**, *133*, 4625.
(7) Small, C. E.; Chen, S.; Subbiah, J.; Amb, C. M.; Tsang, S.-w.; Lai, T.-h.; Reynolds, J. R.; So, F. *Nat. Photonics* **2011**, *6*, 115.
(8) He, Z.; Zhong, C.; Su, S.; Xu, M.; Wu, H.; Cao, Y. *Nat. Photonics* **2012**, *6*, 591.
(9) Avasthi, S.; Lee, S.; Loo, Y. L.; Sturm, J. C. *Adv. Mater.* **2011**, *23*, 5762.
(10) Oosterhout, S. D.; Wienk, M. M.; Al-Hashimi, M.; Heeney, M.; Janssen, R. A. J. *J. Phys. Chem. C* **2011**, *115*, 18901.
(11) Ren, S.; Chang, L. Y.; Lim, S. K.; Zhao, J.; Smith, M.; Zhao, N.; Bulovic, V.; Bawendi, M.; Gradecak, S. *Nano Lett.* **2011**, *11*, 3998.
(12) Xu, T.; Qiao, Q. *Energy Environ. Sci.* **2011**, *4*, 2700.
(13) Liao, H.-C.; Lee, C.-H.; Ho, Y.-C.; Jao, M.-H.; Tsai, C.-M.; Chuang, C.-M.; Shyue, J.-J.; Chen, Y.-F.; Su, W.-F. *J. Mater. Chem.* **2012**, *22*, 10589.
(14) Syu, H.-J.; Shiu, S.-C.; Lin, C.-F. *Sol. Energy Mater. Sol. Cells* **2012**, *98*, 267.
(15) Li, C.-Y.; Wen, T.-C.; Lee, T.-H.; Guo, T.-F.; Huang, J.-C.-A.; Lin, Y.-C.; Hsu, Y.-J. *J. Mater. Chem.* **2009**, *19*, 1643.
(16) Sun, Y.; Gong, X.; Hsu, B. B. Y.; Yip, H.-L.; Jen, A. K. Y. *Appl. Phys. Lett.* **2010**, *97*, 193310.
(17) Espinosa, N.; Dam, H. F.; Tanenbaum, D. M.; Andreasen, J. W.; Jørgensen, M.; Krebs, F. C. *Materials* **2011**, *4*, 169.

(18) Søndergaard, R.; Manceau, M.; Jørgensen, M.; Krebs, F. C. *Adv. Energy Mater* **2012**, *2*, 415.
(19) Xu, Z.; Chen, L.-M.; Yang, G.; Huang, C.-H.; Hou, J.; Wu, Y.; Li, G.; Hsu, C.-S.; Yang, Y. *Adv. Funct. Mater.* **2009**, *19*, 1227.
(20) Bi, D.; Wu, F.; Qu, Q.; Yue, W.; Cui, Q.; Shen, W.; Chen, R.; Liu, C.; Qiu, Z.; Wang, M. *J. Phys. Chem. C* **2011**, *115*, 3745.
(21) Ma, H.; Yip, H.-L.; Huang, F.; Jen, A. K. Y. *Adv. Funct. Mater.* **2010**, *20*, 1371.
(22) Steim, R.; Kogler, F. R.; Brabec, C. J. *J. Mater. Chem.* **2010**, *20*, 2499.
(23) Tan, Z.; Zhang, W.; Zhang, Z.; Qian, D.; Huang, Y.; Hou, J.; Li, Y. *Adv. Mater.* **2012**, *24*, 1476.
(24) Yang, L.; Sontag, S. K.; LaJoie, T. W.; Li, W.; Huddleston, N. E.; Locklin, J.; You, W. *ACS Appl. Mater. Interfaces* **2012**, *4*, 5069.
(25) Yu, J.; Shen, T.-L.; Weng, W.-H.; Huang, Y.-C.; Huang, C.-I.; Su, W.-F.; Rwei, S.-P.; Ho, K.-C.; Wang, L. *Adv. Energy Mater.* **2012**, *2*, 245.
(26) Huang, Y.-C.; Hsu, J.-H.; Liao, Y.-C.; Yen, W.-C.; Li, S.-S.; Lin, S.-T.; Chen, C.-W.; Su, W.-F. *J. Mater. Chem.* **2011**, *21*, 4450.
(27) Hau, S. K.; Yip, H.-L.; Ma, H.; Jen, A. K. Y. *Appl. Phys. Lett.* **2008**, *93*, 233304.
(28) Hau, S. K.; Cheng, Y.-J.; Yip, H.-L.; Zhang, Y.; Ma, H.; Jen, A. K. Y. *ACS Appl. Mater. Interfaces* **2010**, *2*, 1892.
(29) Cheng, Y.-J.; Cao, F.-Y.; Lin, W.-C.; Chen, C.-H.; Hsieh, C.-H. *Chem. Mater.* **2011**, *23*, 1512.
(30) Kyaw, A. K. K.; Sun, X. W.; Jiang, C. Y.; Lo, G. Q.; Zhao, D. W.; Kwong, D. L. *Appl. Phys. Lett.* **2008**, *93*, 221107.
(31) Sun, Y.; Seo, J. H.; Takacs, C. J.; Seifter, J.; Heeger, A. J. *Adv. Mater.* **2011**, *23*, 1679.
(32) Oosterhout, S. D.; Wienk, M. M.; van Bavel, S. S.; Thiedmann, R.; Koster, L. J. A.; Gilot, J.; Loos, J.; Schmidt, V.; Janssen, R. A. J. *Nat. Mater.* **2009**, *8*, 818.
(33) Krüger, B. J.; Bach, U.; Grätzel, M. *Adv. Mater.* **2000**, 447.
(34) Park, J. S.; Lee, B. R.; Lee, J. M.; Kim, J.-S.; Kim, S. O.; Song, M. H. *Appl. Phys. Lett.* **2010**, *96*, 243306.
(35) Becke, A. D. *J. Chem. Phys.* **1993**, *98*, 5648.
(36) Lee, C.; Yang, W.; Parr, R. G. *Phys. Rev. B* **1988**, *37*, 785.
(37) Duan, C.; Cai, W.; Huang, F.; Zhang, J.; Wang, M.; Yang, T.; Zhong, C.; Gong, X.; Cao, Y. *Macromolecules* **2010**, *43*, 5262.
(38) Goh, C.; Scully, S. R.; McGehee, M. D. *J. Appl. Phys.* **2007**, *101*, 114503.
(39) Perez, M. D.; Borek, C.; Forrest, S. R.; Thompson, M. E. *J. Am. Chem. Soc.* **2009**, *131*, 9281.
(40) Yang, L.; Zhou, H.; You, W. *J. Phys. Chem. C* **2010**, *114*, 16793.
(41) Lin, Y. Y.; Chu, T. H.; Li, S. S.; Chuang, C. H.; Chang, C. H.; Su, W. F.; Chang, C. P.; Chu, M. W.; Chen, C. W. *J. Am. Chem. Soc.* **2009**, *131*, 3644.
(42) Thompson, B. C.; Kim, Y.-G.; McCarley, T. D.; Reynolds, J. R. *J. Am. Chem. Soc.* **2006**, *128*, 12714.
(43) Hau, S. K.; Yip, H.-L.; Acton, O.; Baek, N. S.; Ma, H.; Jen, A. K. Y. *J. Mater. Chem.* **2008**, *18*, 5113.